ADVANCED OPTICAL MATERIALS
www.advopticalmat.de

Enhanced Electro-Optic Properties of Blue Phase Liquid Crystals Using Slippery Polymer Stabilization

*Srinivas Pagidi, Venkata Sai Dasari, KP Zuhail, Dan Luo, Surajit Dhara, and Ramesh Manda**

Blue-phase liquid crystals (BPLCs) are promising for next-generation fast-switching displays due to their unique nanoscale self-assembly and soft-crystalline properties. However, conventional stabilization methods using high glass-transition temperature (T_g) polymers, such as acrylates or thiols, often result in high operating voltages due to strong surface anchoring at the LC-polymer interface, limiting practical applications. This study proposes using poly(hexyl methacrylate) (PHMA), a low-T_g polymer (∼−5 °C), to create a slippery polymer network that reduces operating and threshold voltages. Additionally, this sliding interface promotes the BP-III phase, further decreasing the operating voltage to 38% with minimal hysteresis and increasing the relative Kerr constant by ninefold. The biphasic interaction between BPLCs and PHMA is quantitatively analyzed, offering insights into the sliding surface mechanism and optimized the Kerr and response time equations. These findings highlight significant potential for advancing next-generation electro-optic and tunable photonic systems.

1. Introduction

The liquid crystals (LC) manifest diverse anisotropic physical properties, including optical, dielectric, and visco-elastic anisotropy, due to their positional and orientational anisotropy. These properties can be controlled by a variety of external stimuli such as temperature, electric field, magnetic fields, surface morphology, and chemical treatments, enhancing their versatility for applications ranging from displays to non-display technologies like light shutters, spatial light modulators, and photonic applications.[1–5] Over time, synthesis efforts have yielded a variety of LC shapes and structures, leading to the discovery of novel phases and expanded applications. Among the numerous LCs, blue-phase liquid crystals (BPLC) are notable for their nanoscale self-assembly and cubic crystallinity that provide submillisecond response time, wide viewing angle, and light modulation applications.[6–10] External stimuli, such as thermal, optical, electric, and magnetic fields, can tune these structures, promising diverse soft photonic applications.[11,12]

BPLCs exhibit three phases: the amorphous BP-III and cubic crystalline BP-I and BP-II with a few hundred nanometers lattice constant.[13–15] Due to the cubic crystalline lattice, BP-I and BP-II show strong selective reflection, while BP-III appears light blue foggy color due to a lack of selective reflection. BP-III possesses a quasiperiodic structure. These BPLC phases form through the self-assembly of double twist cylinders (DTC), which are building blocks of strongly twisted LC, but the presence of disclination lines between DTCs limits stability to narrow temperature ranges. To overcome this, strategies include using low-molecular-weight BPLCs, introducing quantum dots and nanoparticles, and dispersing various molecular shapes like T-shaped, U-shaped, and hydrogen-bonded molecules.[16–19] These strategies aim to enhance phase stability and broaden the operational temperature range of BPLC. However, these approaches unavoidably introduce unwanted photonic effects.

Another strategy involves dispersing UV-curable monomers into the BPLC and polymerizing them to stabilize the BPLC phase, known as polymer-stabilized BPLC (PS-BPLC).[20,21] This method creates a polymer network within the disclinations without disrupting the local ordering of LC, providing 3D confinement to the cubic lattice and enhancing thermal stability. In addition to enhancing the thermal stability of the phase, it is possible to accomplish large-scale monodomain alignment of cubic lattices, which can be employed in photonics devices and optical elements.[22–25] Furthermore, the intrinsic properties of prepolymers, such as functionality, molecular structure, and glass-transition temperature (T_g), can be easily adjusted to optimize the polymerization and, consequently, the thermal stability of BPLC.

S. Pagidi, D. Luo
Department of Electrical and Electronic Engineering
Southern University of Science and Technology
Nanshan District, Shenzhen, Guangdong 518055, China
V. S. Dasari
Department of Physics
VNR Vignana Jyothi Institute of Engineering and Technology
Bachupally, Nizampet, Hyderabad, Telangana 500090, India
K. Zuhail
Department of Physics
University of Calicut
Thenhipalam, Kerala 673635, India
S. Dhara, R. Manda
Department of Physics
University of Hyderabad
Gachibowli, Hyderabad, Telangana 500046, India
E-mail: manda_rff@uohyd.ac.in

The ORCID identification number(s) for the author(s) of this article can be found under https://doi.org/10.1002/adom.202500778

DOI: 10.1002/adom.202500778

For instance, high T_g prepolymer trimethylolpropane triacrylate (TMPTA, T_g > 200°C) offers a rigid polymer network, providing stronger LC anchoring.[26] In this aspect, a templated BPLC was also developed and demonstrated efficient light modulators, mirrorless lasers, and hyper-reflective films.[11,27–29] However, these polymers form a rigid polymer network, resulting in high operating voltages and unwanted reflections, which are undesirable for practical device applications. A slight modification to this template by incorporating chiral monomers that form the polymer network within the DTC yields room temperature BPLC, though monomer extraction is laborious.[30] Owing to the exotic properties of BPLC, it is crucial to research versatile polymerization techniques that offer superior thermal and electro-optical characteristics. Although the utilization of a sliding polymer interface, particularly in the vicinity of the polymer's T_g, is a known technique to address the high operating issue, it remains limited to conventional modes.[31–34] Using a slippery polymer network to stabilize the BPLC structure remains unexplored in this context.

In our quest to find suitable microstructures for optimizing BPLC stability, we developed a PS-BPLC system stabilized by the slippery prepolymer PHMA (poly(hexyl methacrylate)). The low T_g of PHMA induces a low symmetric BP-III phase, thereby reducing the driving voltage to 25 V (38%). Additionally, this hysteresis-free system exhibits a Kerr constant nine times higher than conventional polymer stabilization. Further, the underlying switching mechanism of slippery polymer stabilized BPLC by analyzing the phase diagram and optimized for higher efficiency. Our study demonstrates the fabrication of soft-photonic lattices with excellent electro-optical properties that offer practical PS-BPLC applications.

2. Materials and Methods

The BPLC was fabricated by mixing a right-handed chiral dopant R5011 (helical-twisting power (HTP) = 126 μm^{-1}, from HCCH) with the eutectic nematic LC mixture, BL002 (nematic-to-isotropic transition temperature (T_{NI}) is 72°C, dielectric anisotropy (Δε) is 17.2 at 1 kHz, birefringence (Δn) is 0.246 at 589.3 nm, phase sequence is Iso 72°C N -20°C Cr, Iso: Isotropic temperature, N: Nematic phase, Cr: Crystalline phase, purchased from Sigma-Aldrich). To stabilize the phase, photopolymers RM257 (from Merck), IBMA (Isobornyl methacrylate, refractive index (n_p) is 1.477, from Sigma-Aldrich), TMPTA (Trimethylolpropane triacrylate, n_p is 1.474, density is 1.1 gmL^{-1} at 25°C, from Sigma-Aldrich), and PHMA polymer (n_p is 1.481, density is 1.007 gmL^{-1} at 25°C, from Sigma-Aldrich) were added. RM257 exhibits a nematic phase from 68.7°C to 128.2°C.[30] TMPTA, a tri-functional acrylate monomer with a high T_g of 225°C, enhances network rigidity, while PHMA, a prepolymer with a low T_g of –5°C, provides a slippery polymer network (Figure S1a, Supporting Information).[34–38] The molecular structures of the utilized material are illustrated in **Figure 1**. PHMA is a colorless viscous liquid at room temperature with a high contact angle (θ_c) of 68° (Figure S1b,c, Supporting Information). The TMPTA is also a colorless liquid with θ_c of 21°. The surface or interfacial tension (σ) was determined using the pendant drop method, as described in Figure S1d,e (Supporting Information). The PHMA exhibits higher surface tension (σ_{PHMA}) of 154 mNm^{-1} compared to TMPTA (σ_{TMPTA} = 58 mNm^{-1}), indicating a weak interaction of surrounding materials.

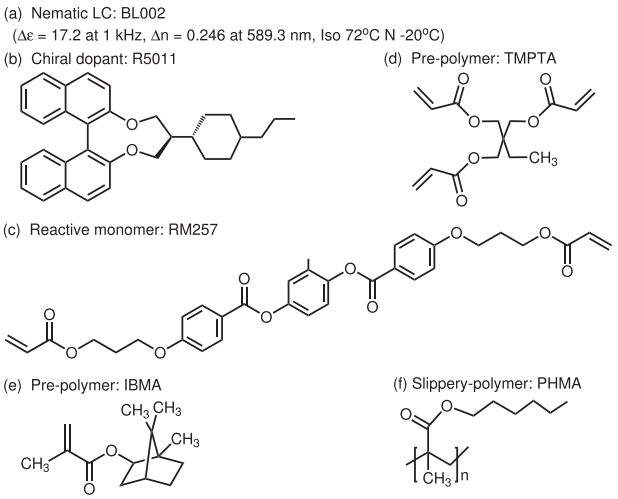

Figure 1. a) Properties of utilized LC, BL-002. Molecular structures of: b) chiral dopant: R5011, c) reactive monomer: RM257, d) prepolymers: TMPTA, e) pre-polymer: IBMA, and f) slippery polymer: PHMA.

3. Results and Discussion

3.1. Phase Studies

The miscibility of PHMA in LC is insufficient.[38] To better understand the interactions and compatibility of these components, we studied the phase diagram of the LC-PHMA binary mixture. The binary phase effect of PHMA on BPLC formation was analyzed as a function of temperature and monomer concentration, with results compared to TMPTA. **Figure 2**a,b depicts the variation in phase transition temperatures with TMPTA and PHMA concentrations in the LC host. Optical textures were recorded during cooling from 85 °C (well above the T_{NI} of LC) at a cooling rate of 0.1°$Cmin^{-1}$. The birefringence of LC allows us to estimate the phase transition temperature based on optical appearance. The BL002 is an eutectic mixture of several nematic LCs with different chain lengths exhibiting a phase sequence of Cr –20 °C N 72 °C I. The investigated system was biphasic, involving only a single monomer (either TMPTA or PHMA) combined with LC, with no additional monomers included. As the optical textures of the sample during phase transition are influenced by abrupt time-dependent thermodynamics, our focus was primarily on changes in phase transition temperature (Figure S2, Supporting Information).

Our study deliberately focuses on phase transition temperatures up to room temperature. The isotropic phase (I), where molecules lack preferred orientation, transitions to the nematic (N) phase, characterized by the Schlieren textures in pristine LC. For LC-TMPTA mixtures, the transition temperature depends on monomer concentration (ϕ_{TMPTA}). The reported transition temperature corresponds to the immediate appearance of the LC phase identified by POM textures that appear colored birefringent textures. At $\phi_{TMPTA} \leqslant 15$ wt%, a direct I-to-N phase transition is observed, indicating minimal disruption to nematic order

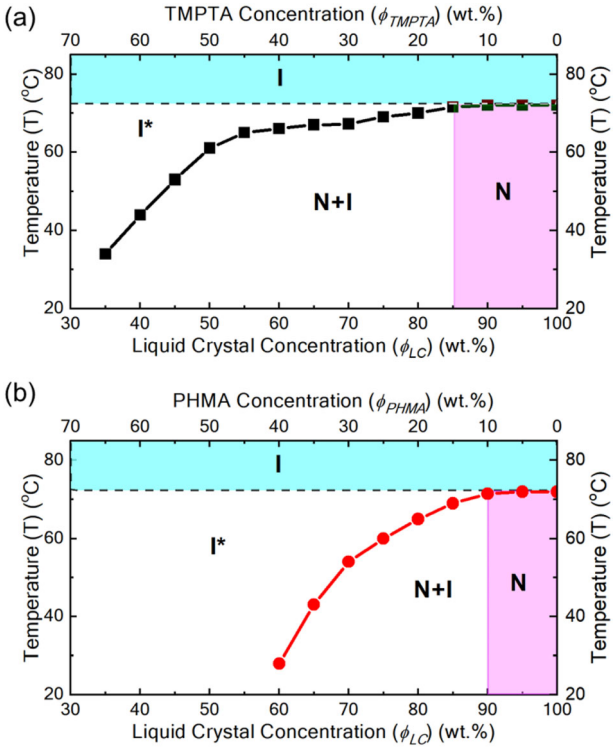

Figure 2. The observed phase transition temperature of: a) LC-TMPTA, b) LC-PHMA. I = Both LC and monomer are in the isotropic phase, I^* = Monomer ordering dominated phase, $N + I$ = Nematic ordering dominated phase. T_{NI} of BL002 is depicted as a dotted line at the top.

(Figure 2a). Beyond 15 wt%, a biphasic I^* region emerges, followed by an $N + I$ region with nematic-dominated coexistence. At higher ϕ_{TMPTA}, phase separation occurs, forming LC droplets within the monomer due to orientational ordering-driven interfacial energy and miscibility differences. Droplet size decreases with further increasing ϕ_{TMPTA}, reaching room temperature transitions at 65 wt%. These results reveal that the reduction in droplet size is primarily due to increased monomer concentration rather than temperature change. This phase separation process, involving coalescence and nucleation growth of LC droplets, takes ~1 min for $\phi_{TMPTA} > 40$ wt%.

A similar trend was noticed for the LC-PHMA system, except the appearance of the I^* occurs after ϕ_{PHMA} of 10 wt% (Figure 2b), which is significantly more rapid than TMPTA. The LC-PHMA system exhibits comparable optical appearances and stability to LC-TMPTA. At $\phi_{PHMA} = 15$ wt%, the Schlieren texture transitioned to stable droplets, with further increase in ϕ_{PHMA} reducing droplet size. This phase transition followed the typical mechanism of nucleation, coalescence, and nucleation growth. The transition temperature dropped rapidly to 29 °C at $\phi_{PHMA} =$ 40 wt.%, exceeding room temperature with further increase. Notably, PHMA exhibits a broader I^* phase region than the TMPTA, indicating stronger dominance of the I^* phase likely due to its presumed weaker interaction with the LC. This phenomenon is ascribed to the linear and elongated flexible hexyl groups of the PHMA polymer, as illustrated in Figure 2f, which reduce surface interactions with the LC molecules, hence enhancing the I^* phase in the composite system compared to the high miscible (and low σ) TMPTA.

To gain more insights, we applied the Flory–Huggins lattice theory combined with Maier–Saupe mean-field theory to this system. The total free energy density (g) of the LC-monomer biphasic system depends on the volume fraction of the LC (ϕ_{LC}) and monomer (ϕ_M), the nematic orientational order parameters (S_{LC}), the isotropic interaction parameter (χ), and the nematic interaction parameter (υ_{LC}) (Section S2, Supporting Information).[39–42] The free energy density of isotropic monomer (g^i) and anisotropic LC (g^{LC}) are influenced by the interaction parameters χ and υ_{LC}. Since the nematic LC is identical in both samples, S_{LC} remains constant, and the I^* phase expansion is solely driven by the polymer's interaction parameter. The χ determines miscibility, υ_{LC} controls interfacial and anchoring energy. Assuming equal molecular weights for both monomers, one possible way to interpret differences in transition temperatures is the attribution of lower χ and υ_{LC}. Therefore, PHMA's low T_g is likely to reduce anchoring strength (low υ_{LC}) and miscibility (low χ), destabilizing nematic order more effectively than TMPTA and significantly lowering g^{LC}.

3.2. BPLC Phase Stabilization

The experimental procedures of BPLC and PS-BPLC fabrication have been previously reported.[30,43] The BPLC mixture consists BL002 (76.7 wt.%), R5011 (2.3 wt.%), RM257 (5 wt.%), IBMA (5 wt.%), and Irgacure-1173 (0.5 wt.%). Two BPLC samples were prepared: S1 with 10.5 wt.% high T_g TMPTA and S2 with 10.5 wt.% low T_g PHMA, to evaluate the impact of monomer's weak surface anchoring interaction, induced by the T_g on the BPLC stability. Both samples, identical except for the targeted monomers, were treated under the same conditions. The monomer concentrations were selected based on their phase behaviors with BL002, where the TMPTA showed no effect on transition temperature, and PHMA had a slight effect. The LC and chiral dopant were mechanically mixed (10 min), sonicated (5 min), and combined with monomers and a photo-initiator. The mixture was then infiltrated into an experimental cell at 85 °C by capillary action, followed by phase identification and phase stabilization by UV light exposure.

Next, the BP phase ranges of S1(TMPTA) and S2(PHMA) were identified using POM, as shown in **Figure 3**. For S1(TMPTA) (Figure 3a), the I^* phase spanned 72 °C to 67.9 °C. The BP-II phase with green and red platelets ranged from 67.9 °C to 67.7 °C (0.2 °C), followed by BP-I with three primary colors from 67.7 °C to 63.9 °C (3.8 °C). After phase stabilization (Figure 3b), the BP-II extended to 9.0 °C (67.9 °C to 58.9 °C) with large green platelets, and BP-I expanded to 30.5 °C (58.9 °C to 28.4 °C) with large red and yellow platelets. For S2 (PHMA) (Figure 3c), we achieved 3.4 °C BP-II (60.4 °C to 57 °C) and 4.6 °C BP-I (57 °C to 52.4 °C). The BP-II consists mostly of blue platelets and fewer yellow platelets, while BP-I consists of red, green, and yellow platelets. Due to the absence of selective reflection of BP-III, the formation of the BP-III phase is unclear. After phase stabilization (Figure 3d), we achieved a 10.5 °C BP-II (59.5 °C to 49 °C) and 16.2 °C BP-I (49 °C to 32.8 °C). Phase stabilization significantly improved the thermal stability of both samples. This implies that the PHMA effectively occupied disclination lines without disrupting the local

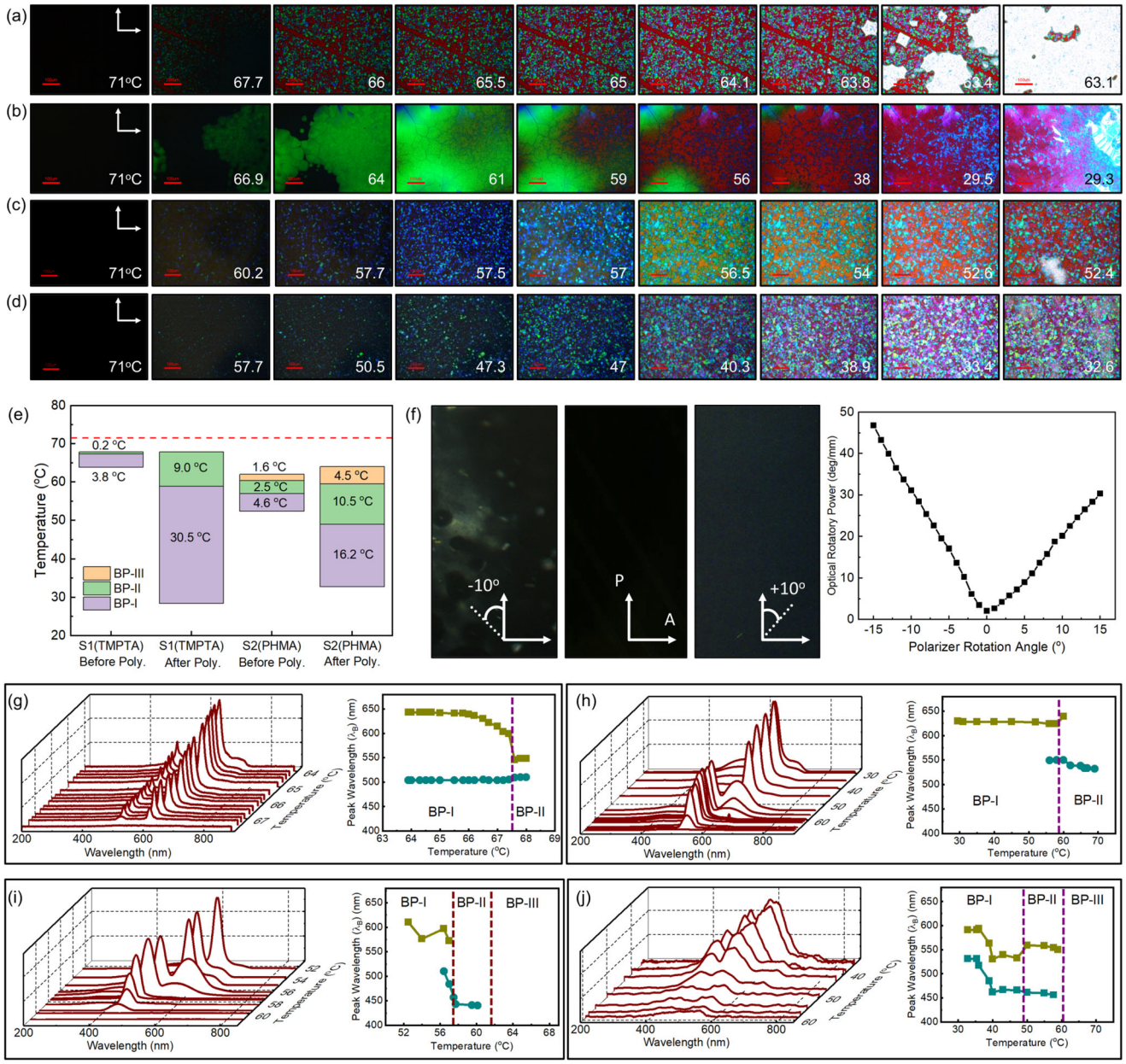

Figure 3. a,b) Optical textures of S1(TMPTA): a) before phase stabilization, b) after phase stabilization. c,d) Optical textures of S2 (PHMA): c) before phase stabilization, d) after phase stabilization. The white arrows denote the polarizer's and analyzer's orientation. Temperatures are indicated as the number on each image. The scale bar is 100 μm. e) Relative phase range of S1(TMPTA) and S2(PHMA) before and after phase-stabilization. The dotted line indicates the T_{NI} of nematic LC. f) BP-III phase identification by optical texture at polarizer rotation of −10°, 0°, and +10°, with relative optical rotatory power plotted against polarizer rotation angle. The white dotted line indicates the polarizer's rotation angle. g–j) Bragg reflection spectra and the associated reflection wavelengths of S1(TMPTA): g) before, and h) after phase-stabilization, and S2(PHMA): i) before, and j) after phase-stabilization. The purple dotted lines indicate the BP-II to BP-I transition.

twisting, similar to TMPTA. Remarkably, a wider BP-III phase emerged after phase stabilization of S2(PHMA), as revealed by optical textures forming before 59.5 °C.

The relative phase existences of both samples before and after phase stabilization are shown in Figure 3e. Notably, the TMPTA-LC system exhibits only BP-I and BP-II phases, while the PHMA-LC system includes BP-III in addition to BP-I and BP-II. The gap between the phase BP-III and T_{NI} of utilized nematic LC was believed to be an I^* phase. Both S1(TMPTA) and S2(PHMA) exhibit the I^* phase, but I^* is more pronounced in S2(PHMA).

Due to the absence of selective reflection, the BP-III phase appears gray and is difficult to identify optically. Its amorphous nature arises from the randomness of DTCs. Although randomly distributed DTCs prevent selective reflection, short-range order makes the phase optically active at short wavelengths under certain conditions. The polarizer rotation technique is the most

effective method to identify this.[44–47] As shown in Figure 3f, the sample appears uniform gray under crossed polarizers. When the polarizer rotated 10° anticlockwise, the texture turned a bluish hue, whereas a 10° clockwise rotation resulted in a different color with reduced intensity. The polarization state of transmitted light is modulated between ±10°, indicating optical activity. An optically isotropic material would exhibit no such variation with polarizer rotation. This optical activity to BP-III could originate from short-range DTC organisation. This is supported by optical rotatory power measurements as a function of polarizer rotation angle up to a maximum of ±10°. The optically isotropic phase should yield symmetric optical rotatory power for both directions. But, a 35% difference in optical rotatory power was observed for both clockwise and anticlockwise rotations, indicating optical activity. This asymmetry, along with differing textures, confirms the presence of a random arrangement of DTC in the BP-III phase.

The dispersed PHMA apparently stabilizes the BP-III phase to some extent (~4.5 °C). The existence of the induced BP-III phase is clearly due to PHMA. In BPLC, disclinations dominate the self-assembly of DTCs, where monomers preferentially occupy these disclination lines and interact strongly with LC molecules. From this, one could anticipate that PHMA's slippery behavior either induced a metastable *I** phase with ordered DTCs or destabilized the cubic phase by promoting DTC sliding, thereby promoting BP-III formation. The latter mechanism is more plausible, suggesting that the BP-III phase arises from the slippery polymer network formed by PHMA.

It is well-known that the Mosoic colors are Bragg reflections (λ_B) from the cubic crystalline planes that can be mathematically expressed as:[6]

$$\lambda_B = \frac{2n_{avg}a\cos\theta_i}{\sqrt{h^2+k^2+l^2}} \quad (1)$$

where n_{avg} is the average refractive index of the nematic LC $\left(=\frac{2n_o+n_e}{3}=1.607\right)$, a is the cubic lattice constant of BPLC, θ_i is angle of incident (= 90°), and (h, k, l) are the Miller indices of cubic lattice. The Bragg reflection spectra for S1(TMPTA) and S2(PHMA) were measured to provide further insights, as shown in Figure 3g–j. The spectra of S1(TMPTA) correlate well with POM textures. The λ_B corresponds to the peak wavelength of reflection. For S1(TMPTA), the BP-II before stabilization showed weak reflection peaks with λ_B of 510 and 550 nm (Figure 3g), while BP-I exhibits λ_B at 510 and ~640 nm. The BP-II to BP-I transition, usually identified as a discontinuity in reflection, is indicated as a dotted line in the inset image. The λ_B depends on the pitch (P) of the BP phase, which can be estimated from $P=\frac{1}{c\times HTP}$, where c is the concentration of the chiral dopant. The estimated P is 345 nm. Considering that the a of BP-I and BP-II equals P and $P/2$, respectively, we further theoretically estimated the reflection plane (hkl) using the Bragg reflection theory described in Supporting Information (Section S3). The obtained 550 nm in BP-II is from the (100) cubic plane and 640 nm in BP-I is from the (110) cubic plane. After phase stabilization (Figure 3h), PS-BPLC showed λ_B at 533 nm (green) for BP-II and 630 nm (red) for BP-I, with a noticeable transition discontinuity. For S2(PHMA) (Figure 3i), BP-II persists at 440 nm (110) and 480 nm (100), while BP-I showed 610 nm (110) reflections, suggesting good PHMA dispersion and selective occupation of disclination lines. After phase stabilization (Figure 3j), the 460 and 550 nm peaks in BP-II are shifted to 530 nm and 590 nm in BP-I, respectively, revealing that the PHMA remains occupied in disclinations after polymerization. The reflection peaks and corresponding Miller indices are summarized in **Table 1**. Theoretically estimated λ_B correlates well with experimental λ_B in BP-II, while some deviation occurs at BP-I. However, this reveals the PHMA is well occupied in disclination lines without disturbing local twisting and self-assembly of DTCs.

The bandwidth ($\Delta\lambda$), defined as the full-width half maximum (FWHM) of a peak, was measured to be 33 nm for BP-II and 30 nm for BP-I in S1(TMPTA). As shown in Table (1), a broader $\Delta\lambda$ of >50 nm was observed across S2(PHMA) spectra. We noticed that this phenomenon is likely attributed to multi-plane reflections and variations in platelet sizes.[48] The average $\Delta\lambda$ estimated for after phase stabilization phase. Additionally, the presence of RM257 in both samples and the existence of BP-III below 68.7 °C indicate that RM257 does not significantly influence BP-III formation.

3.3. Electro-Optical Studies

Next, the switching behavior of S1(TMPTA) and S2(PHMA) was studied under a 1 kHz square wave voltage using POM with crossed polarizers, as shown in **Figure 4**. In BP-I, S1(TMPTA) exhibited induced birefringence (Δn_{Ind}) at the threshold voltage, saturating at 42 V (Figure 4a). The magnitude of Δn_{Ind} was calculated using $\Delta n_{Ind} = \lambda K E^2$, where K is the Kerr constant, λ is the wavelength of the incident light, and E is the applied voltage per unit length. The uniform brightness between electrodes indicates sufficient and homogeneous Δn_{Ind}, without field-induced phase transitions, as the TMPTA network prevented deformation. The switching mechanism involved DTC unwinding and LC reorientation along the field and then elastic relaxation back into the cubic lattice upon voltage removal. Similarly, S2(PHMA) in BP-I exhibited Δn_{Ind} after threshold voltage, which is facilitated by PHMA's slippery polymer network (Figure 4b). This magnifies that the level of induced birefringence is substantially higher for S2 (PHMA) compared to conventional S1(TMPTA) sample, as the uniform fields are applied to both the samples. This enhanced performance could be attributed to weaker surface anchoring interactions between the LC and the well-dispersed low T_g PHMA polymer, which allows the facile unwinding of LC molecules toward the applied field direction within the DTC structure of BPI phase and promotes the effective relaxation during the reassembly of the cubic lattice. Interestingly, S2(PHMA) demonstrated higher Δn_{Ind} in BP-III, attributed to the absence of DTC symmetry and enhanced reorientation dynamics (Figure 4c).

Further, voltage-dependent transmittance of S1(TMPTA) and S2(PHMA) was measured, as shown in Figure 4d. The threshold voltage (V_{Th}) and operating voltage (V_{Op}) were defined as the voltage corresponding to 10% and 90% transmittance, respectively. The measurements were performed in the BP-I phase for S1(TMPTA) and in both BP-I and BP-III phases for S2(PHMA). The Figure 4d,e, revealed that V_{Th} and V_{Op} were 10.5 V and 40 V for S1(TMPTA) and 6.7 and 33.6 V for S2(PHMA) in BP-I. Remarkably, S2(PHMA) achived reduced V_{Th} (4.6 V) and V_{Op}

Table 1. Estimaed (h, k, l), $\Delta\lambda$, and other lattice parameters from Bragg reflection spectra.

Sample	Phase	a[a)] [nm]	λ_B [nm] and [hkl]		λ_B[b)] [nm]	$\Delta\lambda$ nm][c)]
			Before	After		
S1(TMPTA)	BP-I	346	510nm, 640nm (110)	630nm	786	30
	BP-II	173	510nm, 550nm (100)	533nm	556	33
S2(PHMA)	BP-I	346	610nm (110)	530nm, 590nm	786	~50
	BP-II	173	440nm (110), 480nm (100)	460nm, 550nm	556	~60

[a)] Estimated as $a = P$ for BP-I and $a = P/2$ for BP-II. [b)] Theoretically estimated from Equation (1). [c)] Average of after-phase stabilization high-intensity reflection peak.

(24.8 V) in BP-III. Taking half of the $a = P$ for BP-I and $a = \frac{P}{2}$ for BP-II, the anchoring strength (W_a) was estimated from:[49]

$$V_{Th} = l \times \sqrt{\frac{1}{\varepsilon_o \Delta\varepsilon b}\left(\frac{W_a}{2\pi} - \frac{k_{eff}}{\pi b}\right)} \quad (2)$$

where k_{eff} is the effective elastic constant, b is half of the lattice constant (= $a/2$), and l is electrode separation, yielding 9×10^{-4} Nm^{-1} for TMPTA and 4×10^{-4} Nm^{-1} for PHMA in BP-I, with further reduction to 2×10^{-4} Nm^{-1} in BP-III. More than a 50% reduction of W_a was achieved for PHMA. Further, K was calculated by fitting experimental data to the Kerr equation: $\Delta n_{Ind} = \lambda K E^2$. The K was calculated as 0.4 nmV^{-2} for S1(TMPTA), 1.9 nmV^{-2} for S2(PHMA) in BP-I, and 3.8 nmV^{-2} for in BP-III (Figure 4f; Figure S4, Supporting Information). The PHMA network doubled the K in BP-I and further increased to nine times in BP-III, setting a competitive value for superior electro-optic performance.[38,50–52] The K can be described as:[53]

$$K = \Delta n_{Ind} \Delta\varepsilon \left(\frac{\varepsilon_o P^2}{4\pi^2 k_{eff} \lambda}\right) \quad (3)$$

where ε_o is the permittivity of free space. Further, this Equation (3) indicates that K is independent of anchoring strength, which contradicts experimental data. As Δn_{Ind} and $\Delta\varepsilon$, also show no correlation with anchoring strength, an anchoring strength term must be included to this Equation (3) without eliminating the elastic term.

The hysteresis (*Hys*), defined as the voltage difference at 50% transmittance during increasing and decreasing voltage sweeps, was also measured. No indication of residual birefringence. Hysteresis indicates the strength of polymer networks during the LC director reorientation and relaxation. The *Hys* was 1.6 V for S1(TMPTA) and 2.9 V for S2(PHMA) in BP-I, with a reduction to

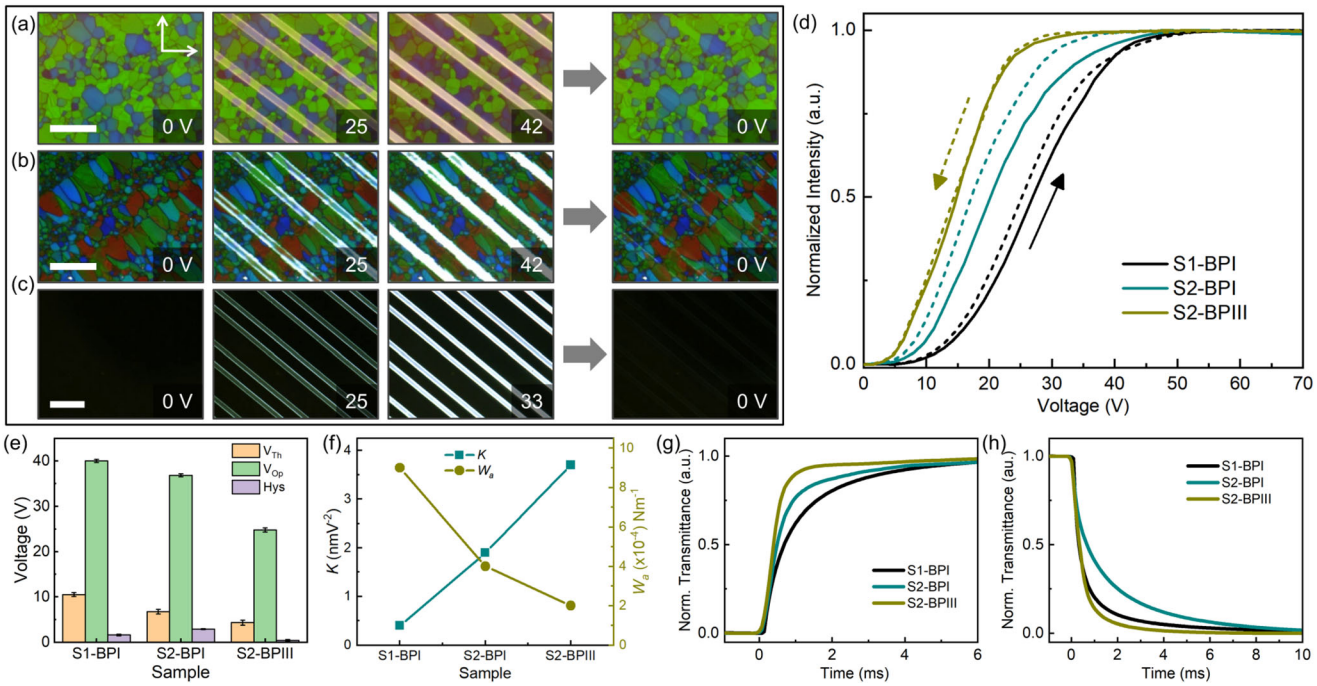

Figure 4. The reversible switching of a) S1 (TMPTA) at BP-I, b) S2 (PHMA) at BP-I, and c) S2 (PHMA) at BP-III. The scale bar is 15 μm. d) Measured voltage-dependent transmittance and hysteresis. The solid arrow indicates voltage increase and the dotted arrow indicates voltage decrease. e) Obtained V_{Th}, V_{Op}, and *Hys*. f) Calculated and W_a. Measured τ_r (g) and τ_d (h).

Table 2. Measured electro-optical properties: K, W_a, τ_r, and τ_d.

Sample	Phase	K [nmV^{-2}]	W_a [Nm^{-1}]	τ_r [ms]	τ_d [ms]
S1(TMPTA)	BP-I	0.4	9×10^{-4}	2.8	3.8
S2(PHMA)	BP-I	1.1	4×10^{-4}	2.1	5.8
	BP-III	3.7	2×10^{-4}	0.9	1.8

0.4 V in BP-III (Figure 4e; Figure S3, Supporting Information). The remarkably negligible *Hys* of the PHMA network is likely due to a sliding interface between the polymer and LC. The visco-elastic coefficients generally govern the director relaxation mechanism. However, our results reveal that the director relaxation dynamics also depend on the surface anchoring energy. To see more insights, we further measured the response time of both samples.

The rise response time (τ_r) and decay response time (τ_d) were measured by applying a square wave voltage and recording the time-dependent transmittance intensity. The τ_r is defined as the time required for director reorientation along the field direction, and it is determined by the amount of dielectric torque. Similarly, the τ_d is the time taken for the director to reassemble into a cubic lattice after the voltage is turned off. Faster τ_r and slower τ_d were observed for PHMA in BP-I, as shown in Figure 4g,h and **Table 2**. From the classical director relaxation time, given by: $\tau_d = \frac{\gamma_1 P^2}{k_{eff} 4\pi^2}$, where γ_1 is rotational viscosity, director relaxation is proportional to the visco-elastic coefficient (γ_1/k_{eff}). In addition to the γ_1, the LC also encounters surface viscosity torque during bulk director relaxation. While this torque may differ from γ_1, we accounted for the resultant viscosity. And, we propose incorporating a sliding anchoring energy term, W_a, to this equation, with $\tau_d \propto 1/W_a$, indicating that weaker anchoring strength (low W_a) results in slower relaxation. In contrast to this trend, BP-III exhibits a faster τ_d. The $\tau_d \propto W_a$ in BP-III. This behavior can be understood as the random DTC distribution contributing to the elastic forces relaxation in this phase. Furthermore, this system has also shown 60% transmission efficiency (Figure S5, Supporting Information), demonstrating the ability of real device applications.

3.4. Morphology Analysis

In the final step, polymer network formation was observed after extracting the LC by immersing the sample in hexane for a few days. The analysis of the polymer network scaffold is also a promising technique for confirming the formation of BP-III.[44–46] As illustrated in **Figure 5**, both S1(TMPTA) and S2(PHMA) samples exhibit polymer network formation due to the selective occupation of polymer molecules in disclination lines. Voids of approximately 250 μm, corresponding to the diameter of DTC, were present in both samples, though it was difficult to estimate the parameter a from the resulting polymer scaffold. The void size is relatively larger compared to Ref. [44, 46]. But, relative void formation indicates formation of BP-III. Remarkably, S1(TMPTA) exhibits uniform polymer strands compared to S2(PHMA). The average strand radius (R_{poly}) was measured at 20 ± 5 μm for S1(TMPTA) and 30 ± 10 μm for S2(PHMA). The higher viscosity of PHMA likely contributed to its less uniform network due to possible local agglomeration. Despite this, S2(PHMA) formed a relatively denser network, which is presumed to have sufficient mechanical strength to resist deformation during the LC extraction.

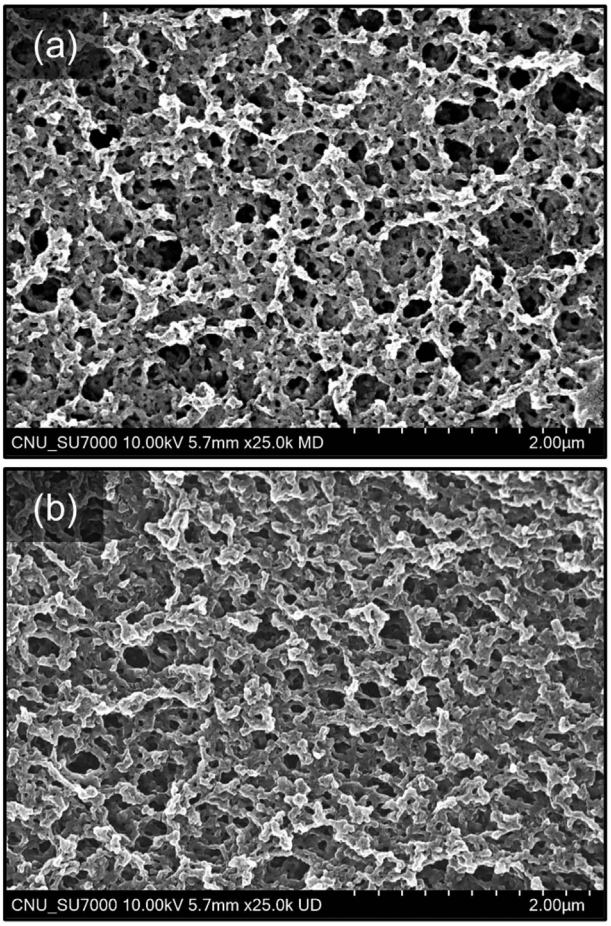

Figure 5. Microstructure of PS-BPLC scaffold of: a) S1(TMPTA), b) S2(PHMA).

4. Discussion

In the DTC model, singular defects with a winding number of −1/2 are present between adjacent DTCs (**Figure 6a**). After phase stabilization, these disclinations are replaced by a polymer network (Figure 6b). The phenomenological free energy of the PS-BPLC system is expressed as:[54]

$$F_{poly} = F_{elas} + F_{thermo} + F_{inter} + F_{surf} \quad (4)$$

where F_{elas}, F_{thermo}, F_{inter}, and F_{surf} represent free energy contributions from elastic deformation, thermodynamic effect, the interfacial tension between the elastic continuum and the polymer network surface, and surface anchoring between the elastic continuum and the polymer network, respectively. Among these, the F_{inter} and F_{surf} play pivotal roles, especially in systems designed to manipulate surface conditions. As the LC molecules radially twist by $-\pi/4$ to $+\pi/4$ across the diameter of DTC, the sliding

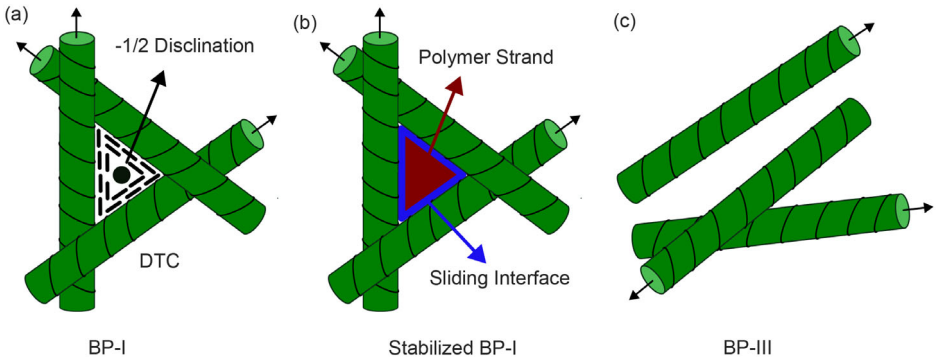

Figure 6. Representation of self-assembly of DTC cylinders in a BP-I: a) Before polymerization, b) after polymerization. c) Random distribution of DTC in BP-III. The polymer network is indicated in red. The blue color indicates the sliding interface.

interface of the polymer network significantly influences both F_{inter} and F_{surf}. The F_{inter} is given by:

$$F_{inter} = 2\sigma\pi R_{poly} \tag{5}$$

where σ is the interfacial tension ($\sigma_{TMPTA} = 68\ mNm^{-1}$, $\sigma_{PHMA} = 164\ mNm^{-1}$), and R_{poly} is the radius of the polymer strand (20 μm for S1(TMPTA) and 30 μm for S2(PHMA)). Based on these findings, calculations yield F_{surf} is $7.2 \times 10^{-6}\ Jm^{-2}$ for TMPTA and $29 \times 10^{-6}\ Jm^{-2}$ for PHMA. Notably, PHMA exhibits a low anchoring energy, which is also influenced by material properties such as the miscibility, length, and flexibility of the side chains. The another term F_{surf} described as:

$$F_{surf} = -\pi R_{poly}(W_p\theta^2 + W_a\varphi^2) \tag{6}$$

where θ and φ are the polar and azimuthal angles, respectively, while W_p and W_a are the corresponding anchoring strengths. These energies quantify the LC anchoring interactions with the polymer network. Given the radial twist of $-\pi/4$ to $+\pi/4$ across the DTC, and considering that the sliding interface may contribute to both W_p and W_a, it is reasonable to assume that $W_p = W_a$ in Equation (6). Thus, we calculated $F_{inter} = 1.41 \times 10^{-8}\ Jm^{-2}$ for TMPTA, decreasing to $0.9 \times 10^{-8}\ Jm^{-2}$ with PHMA in BP-I, and further reduced to $0.47 \times 10^{-8}\ Jm^{-2}$ in BP-III. Although the F_{surf} is higher than F_{inter}, both these terms play a key role in PS-BPLC phase stabilization.

The proposed composites with linear and long hexyl chain polymer demonstrate superior electro-optical properties compared to those of conventional rigid surface polymer systems. Herein, the BP-I of S2(PHMA) doubles the K compared to S1(TMPTA) and further increases it by nine times in BP-III. We believe that the significant enhancement in the system is not solely due to elevated temperatures but also to the weak surface anchoring at the LC-polymer interface. In order to confirm this, we included the anchoring energy term ($K \propto \frac{1}{W_a}$) into the Kerr equation and executed. Consequently, the obtained experimental evidence shows better correlation with Equation (4). In particular, a reduction in W_a by half doubles K. Based on the evidence, we could anticipate that a substantial increase in K by nine times in BPIII phase is possibly attributed to both the weak anchoring surfaces and randomness of DTC self-assembly (Figure 6c). A rigorous simulation study is necessary to analyze the degree of DTC sliding quantitatively.

Unlike BP-I's cubic lattice, which tightly confines LC molecules, BP-III's disordered lattice, free from symmetry and lattice constraints, allows greater reorientation and relaxation of LC molecules, aided by PHMA's slippery interface. This asymmetry enhances the sliding effect, increasing K as LC anchoring does not counteract the dielectric torque due to the electric field ($F_{elec} = \frac{\epsilon_a \Delta\epsilon}{2}(E \cdot n)^2$, E = Electric Field). Additionally, while $\tau_d \propto W_a$, $K \propto \frac{1}{W_a}$, leading to a superior electro-optical performances in the high K system. Based on the enhanced results, we believe that this breakthrough addresses the fundamental challenges of PS-BPLC. The proposed BPLC system stabilized by slippery polymer resulted in a ninefold K increase, a 38% reduction of both V_{Op} and V_{Th}, faster response, and negligible *Hys*. These properties make the system optimal for real-time device applications.

5. Conclusion

We systematically studied two samples of PS-BPLS: one with high T_g and the other with low T_g monomers. Our finding reveals that the low T_g PHMA monomer is promising for addressing short-range phase stability and high driving voltage challenges. The slippery polymer network of low T_g PHMA reduces the interfacial and anchoring free energy, resulting in a significant reduction of the V_{Op} and V_{Th} with doubled Kerr constant. Additionally, the PHMA's slippery polymer network induces the BP-III phase, characterized by lower symmetry and superior electro-optics, further reducing V_{Op} by 38% with negligible *Hys*. The non-symmetric DTC self-assembly of BP-III, combined with a sliding interface, enhances the relative Kerr constant by a remarkable factor of nine. Based on the analytical model, the Kerr equation and response time equation were optimized for PS-BPLC with a slippery interface. This study offers a fundamental insight into better stabilizing BPLC phases through various interactions among distinct polymers, their electro-optical demonstrations, and the potential for diverse photonic applications.

6. Experimental Section

The optical textures of BPLC and PS-BPLC were characterized using a polarizing optical microscope (POM) (Nikon, Eclipse LV100POL). All the

characterizations are carried out as a function of temperature controlled by a precision temperature controller (Instec, MK2000). Phase stabilization was achieved with UV irradiation (20 mW/cm^2 for 10 min) in the BP-I phase. Electro-optics were measured by applying a square-wave voltage through interdigitated patterned electrodes (10 μm and 5 μm width, 5 μm spacing) with a 20 μm cell gap. Bragg reflection peaks were estimated from POM-connected reflection spectra (Ocean Optics, USB2000+), and the reflection level was measured using a UV-visible spectrometer (Jasco, V-760). The microstructure of BPLC is observed using a field-emission scanning electron microscope (ZEISS, Ultra-55).

Supporting Information

Supporting Information is available from the Wiley Online Library or from the author.

Acknowledgements

This work was supported by the Ramanujan Fellowship (RJF/2022/000094), Anusandhan National Research Foundation (ANRF), India. Z.K.P. acknowledges financial support from the Startup Research Grant (SRG/ 2022/1694), Anusandhan National Research Foundation (ANRF), India.

Conflict of Interest

The authors declare no conflict of interest.

Data Availability Statement

The data that support the findings of this study are available from the corresponding author upon reasonable request.

Keywords

blue phase liquid crystals, glass transition temperature, Kerr effect, liquid crystals, slippery polymer

Received: March 10, 2025
Revised: April 12, 2025
Published online: May 13, 2025

[1] I.-C. Khoo, *Liquid crystals*, John Wiley & Sons, Hoboken **2022**.
[2] S. Sato, *Opt. Rev.* **1999**, *6*, 471.
[3] D. H. Kim, Y. J. Lim, D. E. Kim, H. Ren, S. H. Ahn, S. H. Lee, *J. Inf. Display* **2014**, *15*, 99.
[4] I. Abdulhalim, *Liquid Crystals Today* **2011**, *20*, 44.
[5] G. Crawford, *Flexible Flat Panel Displays*, Wiley Series in Display Technology, Wiley, NJ **2005**.
[6] T. Kato, *Liquid crystalline functional assemblies and their supramolecular structures*, vol. *128*, Springer Science & Business Media, New York **2008**.
[7] S. Cho, M. Ozaki, *Symmetry* **2021**, *13*, 1584.
[8] J. Yan, L. Rao, M. Jiao, Y. Li, H.-C. Cheng, S.-T. Wu, *J. Mater. Chem.* **2011**, *21*, 7870.
[9] R. Manda, S. Pagidi, Y. J. Heo, Y. J. Lim, M. S. Kim, S. H. Lee, *Adv. Mater. Interfaces* **2020**, *7*, 1901923.
[10] Y. Wang, H. Cui, Q. Zhao, X. Du, *Matter* **2019**, *1*, 626.
[11] X. Xu, Z. Liu, Y. Liu, X. Zhang, Z. Zheng, D. Luo, X. Sun, *Adv. Opt. Mater.* **2018**, *6*, 1700891.
[12] M. Lopez-Garcia, N. Masters, H. E. O'Brien, J. Lennon, G. Atkinson, M. J. Cryan, R. Oulton, H. M. Whitney, *Sci. Adv.* **2018**, *4*, eaan8917.
[13] Y.-K. Kim, X. Wang, P. Mondkar, E. Bukusoglu, N. L. Abbott, *Nature* **2018**, *557*, 539.
[14] I.-H. Lin, D. S. Miller, P. J. Bertics, C. J. Murphy, J. J. de Pablo, N. L. Abbott, *Science* **2011**, *332*, 1297.
[15] H.-S. Kitzerow, P. Crooker, S. Kwok, J. Xu, G. Heppke, *Phys. Rev. A* **1990**, *42*, 3442.
[16] J. Tang, F. Liu, M. Lu, D. Zhao, *Sci. Rep.* **2020**, *10*, 18067.
[17] S. Yabu, Y. Tanaka, K. Tagashira, H. Yoshida, A. Fujii, H. Kikuchi, M. Ozaki, *Opt. Lett.* **2011**, *36*, 3578.
[18] A. Yoshizawa, M. Sato, J. Rokunohe, *J. Mater. Chem.* **2005**, *15*, 3285.
[19] W. He, G. Pan, Z. Yang, D. Zhao, G. Niu, W. Huang, X. Yuan, J. Guo, H. Cao, H. Yang, *Adv. Mater.* **2009**, *21*, 2050.
[20] H. Kikuchi, M. Yokota, Y. Hisakado, H. Yang, T. Kajiyama, *Nat. Mater.* **2002**, *1*, 64.
[21] R.-Q. Ma, D.-K. Yang, *Phys. Rev. E* **2000**, *61*, 1567.
[22] Q. Chen, X. Wang, C. Xu, H. Chu, H. Yu, C. Ouyang, Y. Lai, Z. Zheng, X. Liang, Y. Lu, et al., *Laser Photonics Rev.* **2024**, *18*, 2301283.
[23] C. Ouyang, Q.-M. Chen, Z.-Y. Xie, C.-T. Xu, Q.-G. Wang, Z.-G. Zheng, D. Luo, Y.-Q. Lu, W. Hu, *Adv. Opt. Mater.* **2024**, 2402844.
[24] Y. Zhang, Z.-G. Zheng, *Appl. Phys. Lett.* **2024**, *125*, 20.
[25] T.-H. Lin, D.-Y. Guo, C.-W. Chen, T.-M. Feng, W.-X. Zeng, P.-C. Chen, L.-Y. Wu, W.-M. Guo, L.-M. Chang, H.-C. Jau, C.-T. Wang, *Nat. Commun.* **2024**, *15*, 7038.
[26] R. Manda, S. Pagidi, M. Kim, C. H. Park, H. S. Yoo, K. Sandeep, Y. J. Lim, S. H. Lee, *Liq. Cryst.* **2018**, *45*, 736.
[27] F. Castles, F. Day, S. Morris, D. Ko, D. Gardiner, M. Qasim, S. Nosheen, P. Hands, S. Choi, R. Friend, et al., *Nat. Mater.* **2012**, *11*, 599.
[28] X. W. Xu, Y. J. Liu, F. Wang, D. Luo, *IEEE Photonics J.* **2018**, *10*, 1.
[29] M. Ravnik, J.-i. Fukuda, *Soft Matter* **2015**, *11*, 8417.
[30] S. Pagidi, R. Manda, S. K. Vishwanath, M.-Y. Choi, M. H. Saeed, S. Dhara, J.-H. Na, *J. Mol. Liq.* **2024**, *398*, 124311.
[31] I. Janossy, T. Kósa, *Phys. Rev. E–Stat., Nonlin. Soft Matter Phys.* **2004**, *70*, 052701.
[32] V. Vorflusev, H.-S. Kitzerow, V. G. Chigrinov, *Appl. Phys. Lett.* **1997**, *70*, 3359.
[33] G. Bryan-Brown, E. Wood, I. Sage, *Nature* **1999**, *399*, 338.
[34] S. Faetti, P. Marianelli, *Liq. Cryst.* **2006**, *33*, 327.
[35] O. Sato, T. Kasai, M. Sato, K. Sakajiri, Y. Tsujii, S. Kang, J. Watanabe, M. Tokita, *J. Mater. Chem. C* **2013**, *1*, 7992.
[36] R. Kizhakidathazhath, H. Higuchi, Y. Okumura, H. Kikuchi, *ChemistrySelect* **2017**, *2*, 6728.
[37] G. Bryan-Brown, E. Wood, I. Sage, *Nature* **1999**, *399*, 338.
[38] S. Pagidi, H. Park, D. Lee, M. Kim, S. H. Lee, *J. Mol. Liq.* **2022**, *350*, 118540.
[39] N. Gogibus, U. Maschke, F. Benmouna, B. Ewen, X. Coqueret, M. Benmouna, *J. Polym. Sci., Part B: Polym. Phys.* **2001**, *39*, 581.
[40] L. Bedjaoui, N. Gogibus, B. Ewen, T. Pakula, X. Coqueret, M. Benmouna, U. Maschke, *Polymer* **2004**, *45*, 6555.
[41] G. W. Smith, *Phys. Rev. Lett.* **1993**, *70*, 198.
[42] T. Kyu, C. Shen, H.-W. Chiu, *Molecular Crystals and Liquid Crystals Science and Technology. Section A. Molecular Crystals and Liquid Crystals* **1996**, *287*, 27.
[43] R. Manda, S. Pagidi, S. S. Bhattacharya, H. Yoo, A. Kumar, Y. J. Lim, S. H. Lee, *J. Phys. D: Appl. Phys.* **2018**, *51*, 185103.
[44] S. S. Gandhi, M. S. Kim, J.-Y. Hwang, L.-C. Chien, *Adv. Mater.* **2016**, *28*, 8998.
[45] H.-Y. Chen, C.-K. Wu, F.-C. Chen, C.-S. Chen, *Liq. Cryst.* **2016**, *43*, 1351.
[46] M. Yamaguchi, K. Shimizu, M. Sagisaka, A. Yoshizawa, *Liq. Cryst.* **2021**, *48*, 54.

[47] H.-C. Jeong, K. V. Le, M.-J. Gim, S.-T. Hur, S.-W. Choi, F. Araoka, K. Ishikawa, H. Takezoe, *J. Mater. Chem.* **2012**, *22*, 4627.
[48] N. Khatun, G. G. Nair, *Chem. Mater.* **2024**, *36*, 4726.
[49] S. Pagidi, A. K. Srivastava, N. Pandey, R. Manda, *J. Mol. Liq.* **2024**, *399*, 124444.
[50] D. Yang, P. Crooker, *Phys. Rev. A* **1988**, *37*, 4001.
[51] R. K. Khan, G. Mohiuddin, N. Begum, S. Turlapati, R. V. Nandiraju, B. K. Debbarma, S. Ghosh, *ACS Appl. Mater. Interfaces* **2022**, *14*, 42628.
[52] K. V. Le, M. Hafuri, H. Ocak, B. Bilgin-Eran, C. Tschierske, T. Sasaki, F. Araoka, *ChemPhysChem* **2016**, *17*, 1425.
[53] P. R. Gerber, *Mol. Cryst. Liq. Cryst.* **1985**, *116*, 197.
[54] M. S. Kim, Ph.D. thesis, Kent State University, **2015**.